Acta Oceanol. Sin., 2024, Vol. 43, No. 9, P. 11–25
https://doi.org/10.1007/s13131-024-2358-z
http://www.aosocean.com
E-mail: ocean2@hyxb.org.cn

Accuracy assessment of global vertical displacement loading tide models for the equatorial and Indian Ocean

Xiaoqing Xu[1, 2, 3], Haidong Pan[1, 2, 3], Fei Teng[1, 2, 3], Zexun Wei[1, 2, 3]*

[1] First Institute of Oceanography, and Key Laboratory of Marine Science and Numerical Modeling, Ministry of Natural Resources, Qingdao 266061, China

[2] Laboratory for Regional Oceanography and Numerical Modeling, Qingdao Marine Science and Technology Center, Qingdao 266237, China

[3] Shandong Key Laboratory of Marine Science and Numerical Modeling, Qingdao 266061, China

Received 24 January 2024; accepted 2 June 2024

Abstract

The three-dimensional displacements caused by ocean loading effects are significant enough to impact spatial geodetic measurements on sub-daily or longer timescales, particularly in the vertical direction. Currently, most tide models incorporate the distribution of vertical displacement loading tides; however, their accuracy has not been assessed for the equatorial and Indian Ocean regions. Global Positioning System (GPS) observations provide high-precision data on sea-level changes, enabling the assessment of the accuracy and reliability of vertical displacement tide models. However, because the tidal period of the K_2 constituent is almost identical to the orbital period of GPS constellations, the estimation of the K_2 tidal constituent from GPS observations is not satisfactory. In this study, the principle of smoothness is employed to correct the systematic error in K_2 estimates in GPS observations through quadratic fitting. Using the adjusted harmonic constants from 31 GPS stations for the equatorial and Indian Ocean, the accuracy of eight major constituents from five global vertical displacement tide models (FES2014, EOT11a, GOT4.10c, GOT4.8, and NAO.99b) is evaluated for the equatorial and Indian Ocean. The results indicate that the EOT11a and FES2014 models exhibit higher accuracy in the vertical displacement tide models for the equatorial and Indian Ocean, with root sum squares errors of 2.29 mm and 2.34 mm, respectively. Furthermore, a brief analysis of the vertical displacement tide distribution characteristics of the eight major constituents for the equatorial and Indian Ocean was conducted using the EOT11a model.

Key words: accuracy assessment, vertical displacement loading tide models, tidal admittance, equatorial and Indian Ocean, GPS constellation

Citation: Xu Xiaoqing, Pan Haidong, Teng Fei, Wei Zexun. 2024. Accuracy assessment of global vertical displacement loading tide models for the equatorial and Indian Ocean. Acta Oceanologica Sinica, 43(9): 11–25, doi: 10.1007/s13131-024-2358-z

1 Introduction

The Earth's deformation caused by the ocean tide loading yields associated gravitational fields. The Vertical Displacement Loading (VDL) tide is generated by the displacement deformation of ocean tides loading (OTL) in the vertical direction, which plays important roles in geodesy, geophysics, and oceanography, and draws widespread attention. VDL tide has irregular spatial patterns that strongly depend on the behaviors of ocean tides around the location of the measurement station and the amplitudes of VDL tide can reach more than tens of centimeters in coastal regions (Yuan et al., 2013; Wei et al., 2022). In the field of oceanography, the vertical displacement loading tide is closely associated with the ocean tide signals obtained from satellite altimeter observations (Fang et al., 2013; Xu et al., 2022). In the field of geophysics, they can also serve as fundamental data for providing sea level corrections across various measurements (Visser et al., 2010) and facilitating accurate vertical datum conversions (Iliffe et al., 2013; Ito et al., 2009).

Global Positioning System (GPS) observations represent the most direct and effective way in which to assess the accuracy of VDL tide models (Shum et al., 1997; Seifi et al., 2019). With advances in observation technology and the methods of data analysis, the number of continuous stations distributed globally has been increasing. This makes the GPS technique be particularly effective in studying tidal vertical displacements, due to the high spatial resolution and precision that are difficult to achieve with other geodetic measurement techniques. As a traditional tool for obtaining VDL tides, GPS measurement stations can provide accurate, verifiable, high-frequency VDL tidal information, especially along coastlines. Harmonic analysis of GPS observations can produce VDL tidal information with high accuracy to the millimeter level. However, they also have some defects, the K_2 tidal constituent obtained from GPS observation analysis is not satisfactory due to their nearly identical tidal periods to the orbital period of the GPS constellation. It is common that the orbital period of the GPS constellation is almost identical to the tidal period of K_2 constituent (11.967 h) (Wei et al., 2019, 2022). Therefore, the estimated tidal harmonic constants of K_2 constituent, obtained through GPS observation data, are obviously inferior to those of other major constituents. This inferiority is attributed to

Foundation item: The Shandong Provincial Natural Science Foundation under contract No. ZR2023QD045; the National Natural Science Foundation of China under contract Nos 42406026, 42076024 and 42106032.
*Corresponding author, E-mail: weizx@fio.org.cn

significant systematic errors (Pan et al., 2023).

The North Indian Ocean is a relatively enclosed sea, mainly connected to the Arabian Sea and the Bay of Bengal through narrow straits. The tides and ocean dynamics in this area are complicated, with the unique topography and geomorphology. Early studies on tides in the Indian Ocean mainly focused on the analysis of measured data and historical data comparison (Aleem, 1967; Pugh, 1979). With the further development and application of ocean numerical models, the understanding of tides in the Indian Ocean has also been deepened (Le Provost and Lyard, 1993; Maraldi et al., 2007; Liu et al., 2019; Wan et al., 2020). So far, the accuracy of the VDL tides in publicly available global ocean tide models has not been evaluated. Given the continuous accumulation of GPS observation data over the years, it is of great significance of using the GPS observations to analyse the accuracy of the VDL tide model.

In response to the above issues, our recent research (Pan et al., 2023) proposed a new method to eliminate the systematic error in GPS observation data and improve the accuracy of K_2 tidal amplitude/phase from GPS observation estimates. Then, This study compared and analyzed the accuracy differences of five VDL tide models (FES2014, EOT11a, GOT4.10c, GOT4.8, and NAO.99b) by using the corrected harmonic constants analyzed from GPS observation data for the equatorial and Indian Ocean.

The structure of our article is as follows: study area and data are provided in Section 2, and methodology is provided in Section 3. Section 4 presents the results of the comparison between VDL tide models and GPS observation results, as well as the VDL tidal characteristics, and limitations of using the GPS observation, followed by the conclusions in Section 5.

2 Study area and data

2.1 *Study area*

Figure 1 shows the bathymetry based on the gridded bathymetric dataset from GEBCO (General Bathymetric Chart of the Oceans). The GEBCO gridded bathymetric dataset is a global terrain model of oceans and lands, providing elevation data in meters at 15 arc-second intervals. These grids can be downloaded or accessed through Web Map Services (https://www.gebco.net).

2.2 *GPS observations data*

In this study, the tidal harmonic constants were obtained from 31 GPS observation data, which was provided by Yuan et al. (2013). The amplitudes and phases of M_2, S_2, N_2, K_2, K_1, O_1, P_1 and Q_1 constituents in the Center of Mass (CM) reference frame are listed in Table 1. Furthermore, the corresponding values in the Center of Figure (CF) reference frame are accurately listed in Table 2. Due to the proximity of some stations, their locations have been rounded to two decimal places, resulting in identical latitudes and longitudes.

2.3 *VDL tide models adopted*

The global VDL tide models used in our study are classified into two categories: one is the empirical model mainly relying on results obtained from satellites (e.g., GOT4.10, GOT4.8, and EOT11a); the other is the assimilation model (e.g., FES2014 and NAO.99b) which are constrained by empirical observations through different assimilation approaches. Table 3 lists the countries, resolutions, major constituents, and types of the five VDL tide models adopted. The details of these models for accuracy assessment are as follows.

The GOT4.10 and GOT4.8 models are developed at Goddard Space Flight Center (GSFC) in the United States and follow a long series of similar efforts starting with Schrama and Ray (Ray, 2013), which are the result of an empirical harmonic analysis of satellite altimetry relative to an adopted prior model. Of the modern models examined here GOT4.10 and GOT4.8 have a spatial resolution of 0.5° × 0.5° with a grid size of 720 × 361, covering latitudes from 90°S to 90°N and longitudes from 0°E–180°–0.5°W. These models provide information on the vertical displacement load tides of 10 constituents in the CM reference frame.

EOT11a is a global empirical ocean tide model obtained through residual analysis of multi-mission satellite altimeter data in 2011 (Savcenko and Bosch, 2012), which is developed at Deutsches Geodtisches Forschungs Institut (DGFI) in Germany. EOT11a is provided on the regular (1/8)° × (1/8)° grid with a grid size of 2 881 × 1 441, covering latitudes from 90°S to 90°N and longitudes from 0°E–180°–0°W. This model provides information on

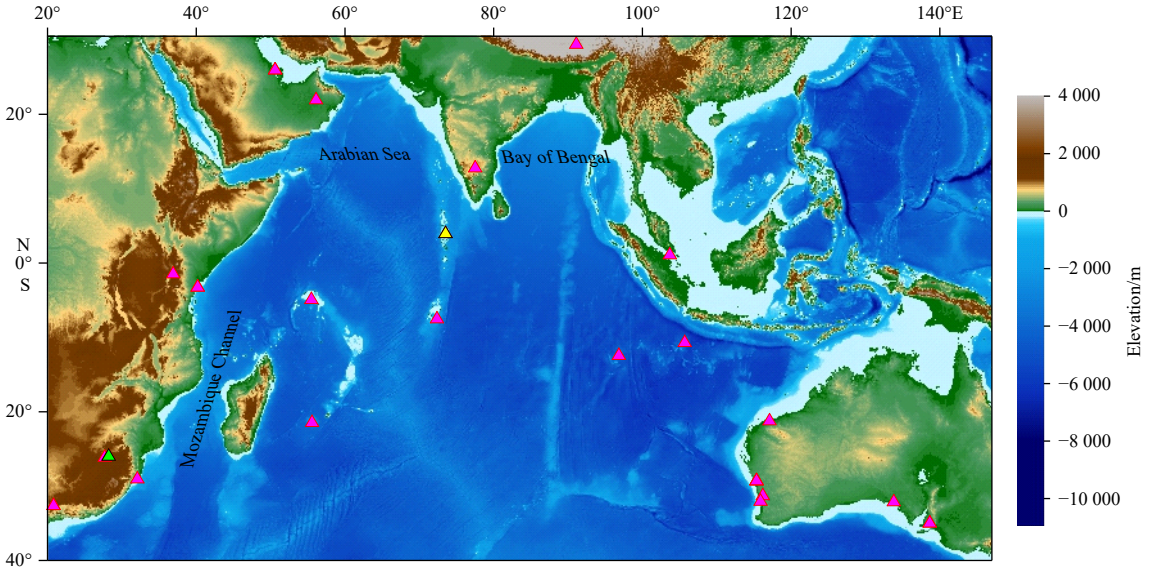

Fig. 1. Distribution of GPS stations in the equatorial and Indian Ocean regions. The triangles denote the 31 GPS stations. The yellow triangle denotes Mald GPS station, and the green triangle denotes Pre2 GPS station.

Table 1. Harmonic constants of eight principal tidal constituents at 31 GPS stations under the CM frame for the equatorial and Indian Ocean

Name	Latitude	Longitude	Duration/d	M_2		S_2		K_1		O_1		N_2		K_2		P_1		Q_1	
				Amp/mm	Pha/(°)	Amp/mm	Pha/(°)	Amp/mm	Pha/(°)	Amp/mm	Pha/(°)	Amp/mm	Pha/(°)	Amp/mm	Pha/(°)	Amp/mm	Pha/(°)	Amp/mm	Pha/(°)
ade1	34.73°S	138.65°E	4 078	1.66	48.9	0.90	343.3	3.43	5.3	4.77	25.4	0.75	56.3	0.73	308.0	2.55	8.2	1.21	21.6
				0.28	9.5	0.28	17.5	0.29	5.0	0.29	3.4	0.28	21.1	0.29	22.3	0.28	6.4	0.29	13.6
ade2	34.73°S	138.65°E	1 787	1.71	47.1	0.63	308.7	3.00	347.3	4.80	25.3	0.80	56.4	1.96	221.0	2.56	17.3	1.19	20.6
				0.41	13.7	0.41	37.1	0.45	7.9	0.42	5.0	0.41	29.4	0.42	12.4	0.42	9.4	0.42	20.3
bahr	26.21°N	50.61°E	4 329	7.62	251.8	3.71	290.8	5.21	185.6	3.25	169.7	1.67	237.3	1.44	312.9	2.54	161.7	0.64	160.4
				0.22	1.6	0.22	3.4	0.24	2.6	0.23	4.0	0.22	7.5	0.23	9.0	0.23	5.1	0.23	20.6
bhr1	26.21°N	50.61°E	3 789	7.59	251.2	3.72	287.7	5.04	184.6	3.24	170.7	1.69	236.0	1.20	298.2	2.54	167.2	0.65	159.9
				0.23	1.7	0.23	3.5	0.24	2.8	0.24	4.2	0.23	7.7	0.23	11.2	0.24	5.3	0.24	20.7
cedu	31.87°S	133.81°E	4 719	0.12	152.2	2.40	284.7	4.81	23.6	4.90	13.8	0.90	37.1	1.18	281.4	1.99	10.0	1.23	12.6
				0.17	80.5	0.17	4.1	0.19	2.2	0.18	2.1	0.17	11.1	0.18	8.7	0.18	5.2	0.18	8.6
coco	12.19°S	96.83°E	5 046	21.36	116.4	9.21	143.8	12.52	326.4	7.78	326.9	4.67	106.1	3.49	145.3	4.21	335.9	1.61	312.6
				0.26	0.7	0.26	1.6	0.28	1.3	0.27	2.0	0.26	3.2	0.27	4.4	0.27	3.7	0.27	9.7
dgar	7.27°S	72.37°E	3 888	28.32	85.1	16.84	112.4	3.98	213.8	3.62	233.2	5.25	81.3	5.83	119.7	1.50	230.6	1.03	221.5
				0.34	0.7	0.34	1.2	0.38	5.5	0.36	5.7	0.35	3.8	0.36	3.5	0.36	13.8	0.36	20.3
hrao	25.89°S	27.69°E	4 882	15.79	226.1	7.97	258.0	2.28	214.5	2.07	186.3	2.96	213.2	2.31	227.3	0.84	205.7	0.43	152.4
				0.21	0.8	0.21	1.5	0.24	6.1	0.23	6.4	0.21	4.2	0.22	5.5	0.23	15.7	0.23	31.1
iisc	13.02°N	77.57°E	4 567	2.40	352.2	2.23	74.2	5.99	156.1	2.42	184.8	0.72	306.1	0.56	335.9	2.07	175.9	0.68	181.2
				0.26	6.2	0.26	6.7	0.30	2.8	0.28	6.6	0.26	20.6	0.27	27.8	0.28	7.8	0.28	23.9
karr	20.98°S	117.10°E	5 293	13.95	232.4	7.54	304.7	9.86	351.2	7.24	340.0	2.42	198.0	2.56	305.6	3.26	338.8	1.67	336.4
				0.20	0.8	0.20	1.5	0.21	1.2	0.21	1.6	0.20	4.7	0.20	4.6	0.21	3.6	0.21	7.2
lhaz	29.66°N	91.10°E	3 886	0.95	239.0	1.36	77.4	2.42	190.7	1.01	207.9	0.45	262.6	1.16	101.4	1.17	147.3	0.30	228.7
				0.23	13.9	0.23	9.6	0.26	6.2	0.25	14.2	0.23	29.7	0.24	11.8	0.25	12.2	0.25	49.1
mal2	3.00°S	40.19°E	1 208	28.61	207.1	13.63	241.4	10.36	197.5	5.46	182.0	5.11	185.7	4.03	252.7	2.90	189.0	1.24	181.2
				0.52	1.0	0.52	2.2	0.55	3.1	0.54	5.7	0.52	5.8	0.54	7.7	0.54	10.6	0.54	25.0
mald	4.19°N	73.53°E	1 284	13.16	59.3	9.30	101.4	8.89	169.8	4.46	191.5	2.06	33.1	2.41	52.0	3.04	168.0	1.57	196.2
				0.82	3.6	0.81	5.0	0.97	6.3	0.90	11.6	0.82	22.8	0.86	20.7	0.90	16.8	0.91	33.1
mali	3.00°S	40.19°E	3 846	28.16	207.4	16.77	238.5	10.02	180.1	5.11	183.3	5.33	189.8	3.61	253.0	2.01	162.6	1.01	175.0
				0.39	0.8	0.40	1.3	0.49	2.9	0.46	5.1	0.40	4.3	0.42	6.6	0.46	12.9	0.46	26.0
nnor	31.05°S	116.19°E	3 404	2.50	83.1	0.67	189.8	9.95	358.2	6.55	358.1	0.90	54.1	0.29	3.4	2.81	343.2	1.55	359.6
				0.27	6.1	0.26	22.8	0.32	1.8	0.30	2.7	0.27	17.1	0.28	54.6	0.30	6.2	0.31	11.4
ntus	1.35°N	103.68°E	3 801	4.21	191.0	1.35	200.5	2.23	342.8	1.98	351.2	1.09	181.1	1.22	112.3	1.05	24.2	0.66	10.7
				0.33	4.6	0.34	14.2	0.36	9.3	0.35	10.0	0.34	17.6	0.35	16.3	0.35	19.0	0.35	30.3
pert	31.80°S	115.89°E	5 436	2.74	79.0	0.62	132.3	9.55	354.2	7.12	358.5	0.95	44.5	0.17	357.6	3.00	351.9	1.51	358.6
				0.20	4.3	0.20	18.9	0.23	1.4	0.23	1.8	0.21	12.3	0.21	72.1	0.22	4.3	0.23	8.6
pre1	25.75°S	28.22°E	4 099	15.78	226.0	8.38	256.4	3.88	225.0	2.02	182.0	3.07	213.8	1.82	245.0	0.70	233.2	0.48	149.7
				0.23	0.8	0.23	1.6	0.24	3.6	0.24	6.7	0.23	4.3	0.24	7.4	0.24	19.4	0.24	28.2
pre2	25.75°S	28.22°E	1 859	15.87	226.0	8.43	250.6	4.03	226.7	1.99	180.0	2.96	215.6	1.78	232.9	1.03	207.2	0.43	157.4

to be continued

continued from Table 1

Name	Latitude	Longitude	Duration/d	M_2		S_2		K_1		O_1		N_2		K_2		P_1		Q_1	
				Amp/mm	Pha/(°)	Amp/mm	Pha/(°)	Amp/mm	Pha/(°)	Amp/mm	Pha/(°)	Amp/mm	Pha/(°)	Amp/mm	Pha/(°)	Amp/mm	Pha/(°)	Amp/mm	Pha/(°)
				0.32	1.1	0.32	2.2	0.34	4.8	0.33	9.4	0.32	6.1	0.33	10.4	0.32	18.1	0.33	43.3
rbay	28.80°S	32.08°E	2 357	26.41	225.2	16.51	253.4	4.23	259.4	2.09	178.0	4.78	214.6	3.68	261.0	0.47	275.7	0.68	138.5
				0.40	0.9	0.40	1.4	0.50	6.8	0.46	12.7	0.41	4.9	0.42	6.7	0.46	55.4	0.47	39.2
rcmn	1.22°S	36.89°E	1 437	11.93	213.4	6.31	233.9	6.27	199.5	3.16	186.0	2.41	199.3	1.90	303.9	2.05	235.3	0.79	169.4
				0.46	2.2	0.46	4.2	0.50	4.6	0.48	8.7	0.46	10.9	0.47	14.6	0.48	13.5	0.48	35.3
reun	21.21°S	55.57°E	3 475	10.26	115.4	1.47	127.8	5.35	242.8	3.15	212.2	2.69	114.4	1.34	110.8	1.72	237.0	0.72	178.6
				0.35	2.0	0.35	13.7	0.41	4.5	0.39	7.1	0.35	7.5	0.37	15.8	0.39	12.9	0.39	31.1
sey1	4.67°S	55.48°E	2 647	20.59	186.5	9.55	223.2	14.24	189.0	7.96	187.6	4.50	168.7	2.91	194.9	3.72	182.8	1.88	180.5
				0.35	2.0	0.35	13.7	0.41	4.5	0.39	7.1	0.35	7.5	0.37	15.8	0.39	12.9	0.39	31.1
suth	32.38°S	20.81°E	4 524	20.25	223.6	8.97	247.5	3.99	233.5	2.00	181.5	4.18	212.7	2.88	248.4	0.89	221.3	0.38	159.5
				0.19	0.5	0.19	1.2	0.20	2.9	0.20	5.6	0.19	2.6	0.19	3.8	0.20	12.5	0.20	29.5
sutm	32.38°S	20.81°E	3 405	20.24	223.9	8.96	246.5	4.95	244.7	1.91	180.1	4.13	212.6	2.61	250.4	0.77	220.2	0.38	166.8
				0.22	0.6	0.22	1.4	0.24	2.7	0.23	6.9	0.22	3.1	0.23	5.0	0.23	17.0	0.23	34.4
xmis	10.45°S	105.69°E	1 822	16.33	168.1	5.38	217.5	11.90	338.8	9.10	331.2	3.99	142.7	1.09	234.5	4.66	345.4	2.10	324.5
				0.49	1.7	0.49	5.2	0.53	2.5	0.51	3.2	0.49	7.1	0.51	26.6	0.51	6.2	0.51	14.0
yar1	29.05°S	115.35°E	2 078	2.58	104.1	0.88	134.4	9.42	352.6	6.71	352.5	0.74	67.8	0.37	162.2	2.94	352.0	1.59	350.4
				0.34	7.5	0.34	21.9	0.39	2.3	0.37	3.1	0.34	26.4	0.35	55.2	0.37	7.1	0.37	13.3
yar2	29.05°S	115.35°E	4 688	2.46	105.6	0.78	190.1	9.39	354.7	6.66	353.1	0.77	69.0	0.30	0.1	3.21	350.2	1.52	351.1
				0.19	4.4	0.19	14.0	0.20	1.3	0.20	1.7	0.19	14.2	0.20	36.9	0.20	3.5	0.20	7.6
yar3	29.05°S	115.35°E	1 476	2.50	109.2	0.18	120.5	8.47	353.9	6.54	353.6	0.87	72.5	0.66	262.4	2.90	343.3	1.53	356.2
				0.36	8.4	0.36	114.6	0.40	2.6	0.38	3.3	0.37	24.1	0.37	32.7	0.38	7.4	0.38	14.2
yarr	29.05°S	115.35°E	2 216	2.41	105.0	0.80	145.4	10.13	353.9	6.64	353.0	0.84	70.2	1.24	248.8	2.68	336.5	1.53	350.7
				0.27	6.5	0.27	19.5	0.29	1.7	0.29	2.5	0.27	18.6	0.28	13.2	0.28	6.1	0.29	10.8
yibl	22.19°N	56.11°E	1 856	6.09	314.6	3.00	328.7	7.67	171.6	5.02	175.7	1.75	300.5	0.53	284.4	3.52	171.0	1.11	179.1
				0.34	3.2	0.34	6.5	0.37	2.8	0.36	4.1	0.34	11.2	0.35	37.6	0.36	5.8	0.36	18.6

Note: Amp represents amplitude, Pha represents Greenwich phase-lag. Corresponding one-sigma formal errors are also listed on the next line.

Table 2. Harmonic constants of eight principal tidal constituents at 31 GPS stations under the CF frame for the equatorial and Indian Ocean

Name	Latitude	Longitude	Duration/d	M_2		S_2		K_1		O_1		N_2		K_2		P_1		Q_1	
				Amp/mm	Pha/(°)	Amp/mm	Pha/(°)	Amp/mm	Pha/(°)	Amp/mm	Pha/(°)	Amp/mm	Pha/(°)	Amp/mm	Pha/(°)	Amp/mm	Pha/(°)	Amp/mm	Pha/(°)
ade1	34.73°S	138.65°E	4 078	1.33	144.5	1.02	294.2	3.87	55.9	5.46	45.1	0.66	93.5	0.85	291.5	2.47	31.6	1.32	32.6
				0.28	9.5	0.28	17.5	0.29	5.0	0.29	3.4	0.28	21.1	0.29	22.3	0.28	6.4	0.29	13.6
ade2	34.73°S	138.65°E	1 787	1.27	142.4	1.17	267.6	2.80	53.1	5.49	44.9	0.70	91.5	2.21	223.0	2.63	39.9	1.29	31.9
				0.41	13.7	0.41	37.1	0.45	7.9	0.42	5.0	0.41	29.4	0.42	12.4	0.42	9.4	0.42	20.3
bahr	26.21°N	50.61°E	4 329	7.48	256.0	3.66	298.8	3.14	192.9	1.74	183.3	1.54	237.9	1.53	316.5	1.85	156.4	0.34	170.2
				0.22	1.6	0.22	3.4	0.24	2.6	0.23	4.0	0.22	7.5	0.23	9.0	0.23	5.1	0.23	20.6
bhr1	26.21°N	50.61°E	3 789	7.44	255.4	3.64	295.6	2.95	191.6	1.75	185.2	1.55	236.4	1.26	303.5	1.83	163.9	0.36	168.9
				0.23	1.7	0.23	3.5	0.24	2.8	0.24	4.2	0.23	7.7	0.23	11.2	0.24	5.3	0.24	20.7
cedu	31.87°S	133.81°E	4 719	2.30	190.1	2.99	273.8	5.83	55.2	5.29	33.6	0.64	66.6	1.38	274.4	2.03	38.5	1.30	23.2
				0.17	80.5	0.17	4.1	0.19	2.2	0.18	2.1	0.17	11.1	0.18	8.7	0.18	5.2	0.18	8.6
coco	12.19°S	96.83°E	5 046	21.65	120.5	9.03	146.2	11.71	338.0	7.79	336.9	4.87	109.7	3.40	148.3	4.09	347.3	1.65	320.3
				0.26	0.7	0.26	1.6	0.28	1.3	0.27	2.0	0.26	3.2	0.27	4.4	0.27	3.7	0.27	9.7
dgar	7.27°S	72.37°E	3 888	27.58	86.5	16.56	112.1	2.08	172.1	2.09	242.8	5.25	83.6	5.67	120.2	0.63	212.6	0.76	229.4
				0.34	0.7	0.34	1.2	0.38	5.5	0.36	5.7	0.35	3.8	0.36	3.5	0.36	13.8	0.36	20.3
hrao	25.89°S	27.69°E	4 882	16.71	229.8	8.01	261.0	2.14	104.9	1.63	114.7	3.10	216.6	2.37	230.4	0.81	112.4	0.43	99.6
				0.21	0.8	0.21	1.5	0.24	6.1	0.23	6.4	0.21	4.2	0.22	5.5	0.23	15.7	0.23	31.1
iisc	13.02°N	77.57°E	4 567	1.93	346.9	2.25	68.9	5.19	140.3	1.27	188.5	0.52	303.9	0.66	330.7	1.63	164.5	0.45	188.9
				0.26	6.2	0.26	6.7	0.30	2.8	0.28	6.6	0.26	20.6	0.27	27.8	0.28	7.8	0.28	23.9
karr	20.98°S	117.10°E	5 293	15.53	227.6	7.86	300.7	9.40	7.0	6.97	351.5	2.81	193.4	2.69	301.5	2.91	353.5	1.68	343.3
				0.20	0.8	0.20	1.5	0.21	1.2	0.21	1.6	0.20	4.7	0.20	4.6	0.21	3.6	0.21	7.2
lhaz	29.66°N	91.10°E	3 886	0.96	199.9	1.45	73.5	1.54	225.1	1.34	266.6	0.24	228.6	1.11	98.4	0.69	143.1	0.41	263.4
				0.23	13.9	0.23	9.6	0.26	6.2	0.25	14.2	0.23	29.7	0.24	11.8	0.25	12.2	0.25	49.1
mal2	3.00°S	40.19°E	1 208	28.73	209.0	13.37	243.0	8.06	187.5	3.91	171.9	5.11	186.6	4.08	254.4	2.24	174.2	0.92	177.4
				0.52	1.0	0.52	2.2	0.55	3.1	0.54	5.7	0.52	5.8	0.54	7.7	0.54	10.6	0.54	25.0
mald	4.19°N	73.53°E	1 284	12.53	60.6	9.15	100.2	7.98	156.3	3.17	187.6	1.99	37.8	2.35	49.1	2.74	155.0	1.32	198.8
				0.82	3.6	0.81	5.0	0.97	6.3	0.90	11.6	0.82	22.8	0.86	20.7	0.90	16.8	0.91	33.1
mali	3.00°S	40.19°E	3 846	28.28	209.3	16.50	239.8	8.37	166.0	3.54	172.6	5.33	190.7	3.67	254.8	1.82	135.0	0.70	167.1
				0.39	0.8	0.40	1.3	0.49	2.9	0.46	5.1	0.40	4.3	0.42	6.6	0.46	12.9	0.46	26.0
nnor	31.05°S	116.19°E	3 404	2.51	133.1	1.20	218.0	9.84	17.5	6.82	14.1	0.76	83.5	0.29	311.2	2.50	5.6	1.66	8.4
				0.27	6.1	0.26	22.8	0.32	1.8	0.30	2.7	0.27	17.1	0.28	54.6	0.30	6.2	0.31	11.4
ntus	1.35°N	103.68°E	3 801	5.60	188.8	1.57	210.1	2.71	15.9	2.50	4.4	1.41	173.3	1.09	116.1	1.42	38.1	0.80	10.7
				0.33	4.6	0.34	14.2	0.36	9.3	0.35	10.0	0.34	17.6	0.35	16.3	0.35	19.0	0.35	30.3
pert	31.80°S	115.89°E	5 436	2.51	126.5	0.72	193.9	9.25	14.8	7.40	13.4	0.73	71.0	0.25	285.8	2.85	13.2	1.61	8.0
				0.20	4.3	0.20	18.9	0.23	1.4	0.23	1.8	0.21	12.3	0.21	72.1	0.22	4.3	0.23	8.6
pre1	25.75°S	28.22°E	4 099	16.69	229.7	8.41	259.2	1.54	156.0	1.76	111.4	3.22	217.0	1.92	248.1	0.55	87.0	0.49	103.3
				0.23	0.8	0.23	1.6	0.24	3.6	0.24	6.7	0.23	4.3	0.24	7.4	0.24	19.4	0.24	28.2
pre2	25.75°S	28.22°E	1 859	16.79	229.7	8.41	253.4	1.49	162.9	1.81	109.8	3.12	218.8	1.85	236.6	0.80	126.0	0.41	102.9

to be continued

continued from Table 2

Name	Latitude	Longitude	Duration/d	M_2		S_2		K_1		O_1		N_2		K_2		P_1		Q_1	
				Amp/mm	Pha/(°)	Amp/mm	Pha/(°)	Amp/mm	Pha/(°)	Amp/mm	Pha/(°)	Amp/mm	Pha/(°)	Amp/mm	Pha/(°)	Amp/mm	Pha/(°)	Amp/mm	Pha/(°)
				0.32	1.1	0.32	2.2	0.34	4.8	0.33	9.4	0.32	6.1	0.33	10.4	0.32	18.1	0.33	43.3
rbay	28.80°S	32.08°E	2 357	27.44	227.3	16.57	254.7	0.72	309.0	2.07	111.3	4.96	216.4	3.82	262.0	0.85	57.4	0.73	106.4
				0.40	0.9	0.40	1.4	0.50	6.8	0.46	12.7	0.41	4.9	0.42	6.7	0.46	55.4	0.47	39.2
rcmn	1.22°S	36.89°E	1 437	12.05	218.0	5.96	237.2	3.97	183.2	1.57	168.6	2.40	201.7	2.01	305.2	1.18	244.3	0.49	156.3
				0.46	2.2	0.46	4.2	0.50	4.6	0.48	8.7	0.46	10.9	0.47	14.6	0.48	13.5	0.48	35.3
reun	21.21°S	55.57°E	3 475	9.48	121.2	1.11	124.3	1.81	228.2	1.34	181.0	2.67	118.6	1.17	112.3	0.61	211.7	0.48	151.9
				0.35	2.0	0.35	13.7	0.41	4.5	0.39	7.1	0.35	7.5	0.37	15.8	0.39	12.9	0.39	31.1
sey1	4.67°S	55.48°E	2 647	20.88	188.6	9.36	225.0	12.40	179.5	6.42	181.5	4.59	169.3	2.88	197.7	3.21	169.6	1.57	177.6
				0.51	1.4	0.50	3.0	0.66	2.7	0.60	4.4	0.51	6.5	0.54	10.6	0.60	9.2	0.61	18.5
suth	32.38°S	20.81°E	4 524	21.18	226.9	8.97	250.0	1.33	163.6	2.01	112.0	4.35	215.6	2.99	250.0	0.67	116.6	0.41	100.0
				0.19	0.5	0.19	1.2	0.20	2.9	0.20	5.6	0.19	2.6	0.19	3.8	0.20	12.5	0.20	29.5
sutm	32.38°S	20.81°E	3 405	21.18	227.1	8.95	249.1	1.35	221.4	2.02	109.1	4.30	215.5	2.72	252.1	0.72	107.8	0.37	104.0
				0.22	0.6	0.22	1.4	0.24	2.7	0.23	6.9	0.22	3.1	0.23	5.0	0.23	17.0	0.23	34.4
xmis	10.45°S	105.69°E	1 822	17.90	170.2	5.78	220.0	11.46	349.6	9.05	338.5	4.36	144.3	1.27	237.9	4.59	354.2	2.15	329.0
				0.49	1.7	0.49	5.2	0.53	2.5	0.51	3.2	0.49	7.1	0.51	26.6	0.51	6.2	0.51	14.0
yar1	29.05°S	115.35°E	2 078	3.23	144.4	0.89	179.0	9.07	12.5	6.82	7.8	0.74	102.4	0.46	195.2	2.81	12.6	1.66	359.2
				0.34	7.5	0.34	21.9	0.39	2.3	0.37	3.1	0.34	26.4	0.35	55.2	0.37	7.1	0.37	13.3
yar2	29.05°S	115.35°E	4 688	3.18	146.6	1.28	215.7	9.15	14.7	6.79	8.5	0.78	102.1	0.31	312.2	3.03	9.1	1.59	0.3
				0.19	4.4	0.19	14.0	0.20	1.3	0.20	1.7	0.19	14.2	0.20	36.9	0.20	3.5	0.20	7.6
yar3	29.05°S	115.35°E	1 476	3.31	148.3	0.58	231.1	8.25	16.0	6.69	9.2	0.89	101.6	0.91	258.4	2.61	4.2	1.62	5.0
				0.36	8.4	0.36	114.6	0.40	2.6	0.38	3.3	0.37	24.1	0.37	32.7	0.38	7.4	0.38	14.2
yarr	29.05°S	115.35°E	2 216	3.13	146.9	0.95	189.6	9.81	12.4	6.76	8.4	0.85	100.3	1.49	248.6	2.28	359.0	1.60	359.8
				0.27	6.5	0.27	19.5	0.29	1.7	0.29	2.5	0.27	18.6	0.28	13.2	0.28	6.1	0.29	10.8
yibl	22.19°N	56.11°E	1 856	6.39	316.2	3.26	335.2	5.70	166.9	3.58	181.4	1.68	303.4	0.60	294.8	2.86	167.7	0.85	187.1
				0.34	3.2	0.34	6.5	0.37	2.8	0.36	4.1	0.34	11.2	0.35	37.6	0.36	5.8	0.36	18.6

Note: Amp represents amplitude, Pha represents Greenwich phase-lag. Corresponding one-sigma formal errors are also listed on the next line.

Table 3. The main properties of the five VDL tide models adopted

Model	Country	Resolution	Type	Major constituent
FES2014	France	(1/16)° × (1/16)°	H	M_2, S_2, K_1, O_1, N_2, P_1, K_2, Q_1, J_1, $2N_2$, L_2, T_2, R_2, Mu_2, Nu_2, La_2, MKS_2, E_2, M_3, N_4, S_4, M_4, MN_4, MS_4, M_6, M_8, M_f, M_m, MS_f, M_{sqm}, M_{tm}, S_a, S_{sa} (total: 33)
EOT11a	Germany	(1/8)° × (1/8)°	E	M_2, S_2, N_2, K_2, K_1, O_1, P_1, Q_1, S_1, $2N_2$, M_f, M_m, M_4 (total: 13)
GOT4.10c	US	(1/2)° × (1/2)°	E	M_2, S_2, K_1, O_1, N_2, P_1, K_2, Q_1, S_1, M_4 (total: 10)
GOT4.8	US	(1/2)° × (1/2)°	E	M_2, S_2, K_1, O_1, N_2, P_1, K_2, Q_1 (total: 8)
NAO.99b	Japan	(1/2)° × (1/2)°	H	M_2, S_2, K_1, O_1, N_2, P_1, K_2, Q_1, M_1, J_1, OO_1, $2N_2$, Mu_2, Nu_2, L_2, T_2, M_f, M_m, MS_f, M_{sm}, M_{tm}, S_a, S_{sa} (total: 23)

Note: E represents empirical model; H represents assimilation model.

the vertical displacement load tides of 13 constituents in the CF reference frame.

FES2014 is the latest finite elements hydrodynamic model, which absorbs tide gauge observations and multi-mission altimeter data which is developed at French Tidal Group (Lyard et al., 2021). FES2014 is based on the resolution of spectral-configured shallow water hydrodynamic equations, and uses global finite element grids with increasing resolution in coastal and shallow water regions, with a spatial resolution of (1/16)° × (1/16)° and a grid size of 5 760 × 2 881, covering latitudes from 90°S to 90°N and longitudes from 0°E–180°–0.062 5°W. This model provides information on the vertical displacement load tides of 33 constituents in the CM reference frame.

NAO.99b model is an assimilation model developed by the National Astronomical Observatory (NAO) in Japan (Matsumoto et al., 2000). It has a resolution of 0.5° × 0.5° with a grid size of 720 × 360, covering latitudes from 89.75°S to 89.75°N and longitudes from 0.25°E–180°–0.25°W. This model provides information on the vertical displacement load tides of 23 constituents in the CM reference frame.

3 Methodology

3.1 *Admittance correction methodology*

Munk and Cartwright (1966) introduced the concept of tidal admittance when proposing the response methodology for tidal analysis. The tidal admittance A_n for a specific constituent n is defined as follows:

$$A_n = A_n^* \exp(-\mathrm{i}g_n), \tag{1}$$

where $A_n^* = H_n/C_n$, with H_n is amplitude and C_n is the coefficient of tidal generating force, and g_n is phase lag.

For the same constituent, the relative admittance of the equilibrium tide with respect to the constituent obtained from GPS analysis can be defined as

$$R_{m/n} = \frac{A_{\mathrm{GPS}}}{A_{\mathrm{equ}}} = \frac{A^*_{\mathrm{GPS}}}{A^*_{\mathrm{equ}}} \exp[-\mathrm{i}(g_{\mathrm{GPS}} - g_{\mathrm{equ}})] = R^*_{\mathrm{GPS/equ}} \exp(-\mathrm{i}r_{\mathrm{GPS/equ}}), \tag{2}$$

where,

$$R^*_{\mathrm{GPS/equ}} = \frac{A^*_{\mathrm{GPS}}}{A^*_{\mathrm{equ}}} = \frac{H_{\mathrm{GPS}}}{H_{\mathrm{equ}}}, \tag{3}$$

$$r_{\mathrm{GPS/equ}} = g_{\mathrm{GPS}} - g_{\mathrm{equ}}, \tag{4}$$

where $R^*_{\mathrm{GPS/equ}}$ represents amplitude ratios, $r_{\mathrm{GPS/equ}}$ represents phase lag.

For any observation point (λ, φ), the corresponding equilibrium tide ζ_{EQ} can be expressed as

$$\zeta_{\mathrm{EQ}} = \sum_{i=1}^{m} f_i H_{\mathrm{equ}_i} \cos\left[\omega_i t + (V_0 + u)_i + (p_i\lambda + \omega_i S)\right], \tag{5}$$

where m is the eight tidal constituents; f_i and u_i are nodal correction factors of the i-th component; V_0 may be expressed by astronomy phase in the corresponding expansion term of tidal potential at $t = 0$ in Greenwich system of the i-th component; ω_i is the frequency of the i-th tidal constituent; p is tide group number, $p = 1$ represents diurnal tide, $p = 2$ represents semi-diurnal tide; λ is longitude; φ is latitude; $S = 0$ represents Greenwich universal time, H_{equ_i} is the theoretical equilibrium amplitude of the i-th constituent corrected by the earth tide, H_{equ} can be expressed as

$$\begin{cases} H_{\mathrm{equ}_{\mathrm{M_2}}} = 0.168\cos^2\varphi, \\ H_{\mathrm{equ}_{\mathrm{S_2}}} = 0.078\ \cos^2\varphi, \\ H_{\mathrm{equ}_{\mathrm{N_2}}} = 0.032\ \cos^2\varphi, \\ H_{\mathrm{equ}_{\mathrm{K_2}}} = 0.021\ \cos^2\varphi, \\ H_{\mathrm{equ}_{\mathrm{K_1}}} = 0.104\ \sin(2\varphi), \\ H_{\mathrm{equ}_{\mathrm{O_1}}} = 0.070\ \sin(2\varphi), \\ H_{\mathrm{equ}_{\mathrm{P_1}}} = 0.033\ \sin(2\varphi), \\ H_{\mathrm{equ}_{\mathrm{Q_1}}} = 0.013\ \sin(2\varphi). \end{cases} \tag{6}$$

Our methodology is based on Pan et al. (2023) which is built on the principle of smoothness about tidal admittance. The method (Pan et al., 2023) is based on the different physical characteristics between non-astronomical tides and astronomical tides. The admittance in a narrow band is similar to astronomical tides, moreover, it can be represented as a smoothing function of the tidal frequency (Zetler, 1971). Through the quadratic interpolation, astronomical K_2 tide can be separated from GPS system errors. Due to the VDL tide is generated by the displacement deformation of OTL in the vertical direction, the tidal responses for the VDL tide inherit the nature of smooth tidal admittance. namely, the tidal admittance for the VDL tide can be represented by the approximate algorithms of smoothing functions of tidal frequencies.

3.2 *Accuracy evaluation methodology*

The tidal constituents obtained from GPS gauge measured data were compared with the corresponding VDL tide model results.

To quantify the error of each tidal constituent between GPS observations and the corresponding VDL tide models, the mean absolute difference values were calculated using the following formula:

$$\begin{cases} \Delta H = \dfrac{1}{N}\sum\limits_{j=1}^{N}\left|H_{\mathrm{mod},j} - H_{\mathrm{obs},j}\right|, \\ \Delta g = \dfrac{1}{N}\sum\limits_{j=1}^{N}\left|g_{\mathrm{mod},j} - g_{\mathrm{obs},j}\right|, \end{cases} \tag{7}$$

where H and g are amplitude and phase, the subscripts mod and obs represent the simulated values of the VDL tide models and the observation values of the GPS gauges, respectively. j represents the serial number of the GPS gauges, N is the number of GPS gauges used, $j = 1, 2, \cdots, N$.

Further, we used the Root-Mean-Square (RMS) value known as the standard deviation, to represent the overall deviation of the VDL tide models and GPS observation values, the RMS value was calculated using the following formula:

$$\mathrm{RMS} = \left\{\frac{1}{N}\sum_{j=1}^{N}\left[\left(a_{\mathrm{mod},j} - a_{\mathrm{obs},j}\right)^2 + \left(b_{\mathrm{mod},j} - b_{\mathrm{obs},j}\right)^2\right]\right\}^{1/2}, \tag{8}$$

where a is the cosine component of the harmonic constant and b is the sine component of the harmonic constant, which are calculated as follows:

$$\begin{cases} a = H\cos g, \\ b = H\sin g. \end{cases} \tag{9}$$

The RMS is the distance between the model simulated value and the actual observed value, representing the degree of deviation between the model simulated value and the actual observed value, while the relative degree of deviation between the RMS and the actual observed value can be expressed as the relative deviation δ,

$$\delta = \mathrm{RMS}/s, \tag{10}$$

where,

$$s = \left\{\frac{1}{N}\sum_{j=1}^{N}\left[\left(a_{\mathrm{obs},j} - \overline{a}_{\mathrm{obs}}\right)^2 + \left(b_{\mathrm{obs},j} - \overline{b}_{\mathrm{obs}}\right)^2\right]\right\}^{1/2}, \tag{11}$$

where $\overline{a}_{\mathrm{obs}}$ represents the average value over all the GPS stations of $a_{\mathrm{obs},j}$, $\overline{b}_{\mathrm{obs}}$ represents the average value over all the GPS stations of $b_{\mathrm{obs},j}$.

We can also use the degree of fit (r^2) between the model values and the actual observed values,

$$r^2 = 1 - \delta^2, \tag{12}$$

where r is equivalent to the correlation coefficient in linear regression.

In addition, the Root-Square-Sum (RSS) value was used to quantify the accuracy of VDL tide models, the RSS value of the m major constituents was calculated by the following formula:

$$\mathrm{RSS} = \left(\sum_{i=1}^{m}\mathrm{RMS}_i^2\right)^{1/2}, \tag{13}$$

where m is the eight tidal constituents mentioned above.

4 Results and discussion

4.1 *Admittance correction results*

According to the tidal theory, the tidal responses for the VDL tide inherit the nature of smooth tidal admittance, the tidal admittance for the VDL tide can be represented by the approximate algorithms of smoothing functions of tidal frequencies, which are here approximated by quadratic functions of tidal frequencies for the normalized amplitudes and phase lags. For the semi-diurnal tidal group, we use the tidal admittances of N_2, M_2, and S_2 constituents and the quadratic interpolation method to determine the interpolated quadratic curves. It is worth noting that K_2 tidal admittances which are contaminated by GPS-system errors are not used. Due to typicality in the poor estimation of K_2 tidal parameters associated with GPS-system errors, Mald (4.19°N, 73.53°E) and Pre2 (25.75°S, 28.22°E) are discussed in detail as the typical examples. As shown in Figs 2 and 3 at Mald GPS station, we calculate the astronomical K_2 admittances (red dots in Figs 2 and 3) by using the quadratic interpolation method for interpolation. Due to the known equilibrium amplitude of the K_2 constituent (as shown in Section 3.1), the amplitude and phase lag of the astronomical K_2 constituent at Mald GPS station can be figured out as 2.66 mm and 104.4° in the CM frame, as 2.63 mm and 103.2° in the CF frame, respectively.

There are two main energy sources for the K_2 tide obtained from GPS observations. One is a consequence of the astronomical K_2 tide generated by astronomical factors, and the other is a consequence of the non-astronomical K_2 tide majorly induced by GPS-system errors. Therefore, Fig. 4 shows the Mald GPS station as an example, the observed K_2 tide (represented by the black arrow) is composed of the vector sum of astronomical K_2 tide (represented by the red arrow) and non-astronomical K_2 tide (represented by the blue arrow). The observed K_2 amplitude and phase lag at the Mald GPS station are 2.41 mm and 52.0° in the CM frame, and 2.35 mm and 49.1° in the CF frame, respectively. The amplitude and phase lag of the astronomical K_2 constituent are 2.66 mm and 104.4° in the CM frame, and 2.63 mm and 103.2° in the CF frame, respectively. Figure 4 clearly indicates that the astronomical K_2 tide is highly consistent with the modeled K_2 tide

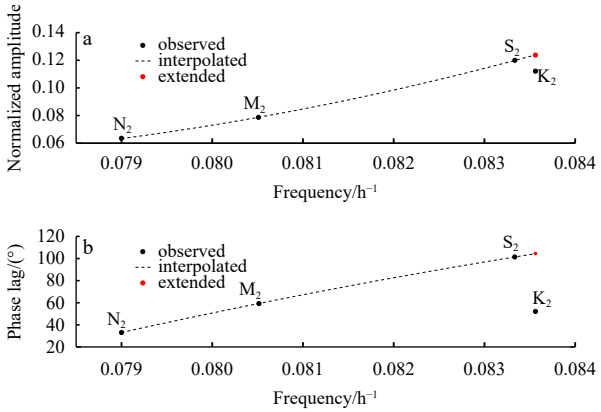

Fig. 2. Tidal admittances of the semi-diurnal VDL tide at Mald station in the CM frame. a. Distribution between normalized amplitudes and the frequency of semi-diurnal constituents. b. Distribution between phase lags and the frequency of semi-diurnal constituents. Black dots signify the observed tidal admittances while the dashed lines indicate the interpolated curves. Red dots denote the extended K_2 values based on the interpolated curves.

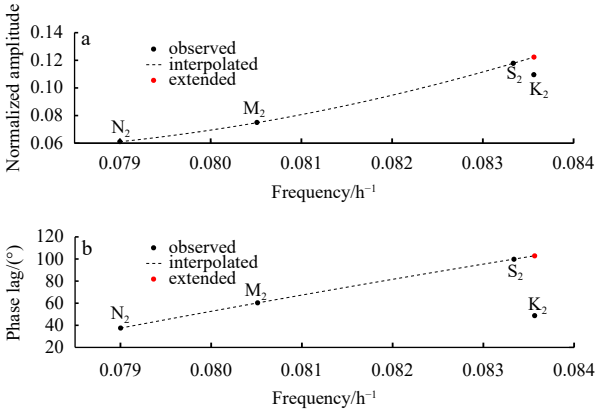

Fig. 3. Tidal admittances of the semi-diurnal VDL tide at Mald station in the CF frame. a. Distribution between normalized amplitudes and the frequency of semi-diurnal constituents. b. Distribution between phase lags and the frequency of semi-diurnal constituents. Black dots signify the observed tidal admittances while the dashed lines indicate the interpolated curves. Red dots denote the extended K_2 values based on the interpolated curves.

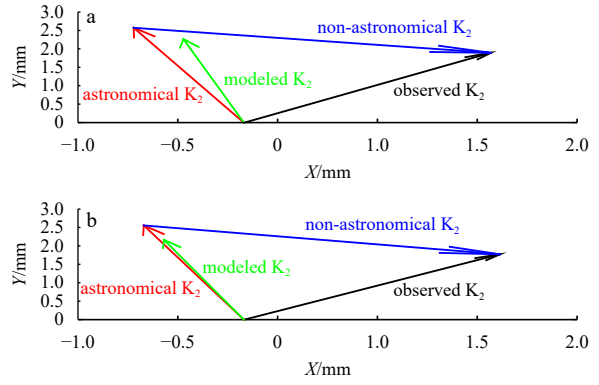

Fig. 4. Vectorial composition of the K_2 constituent of VDL tide. a. Observed K_2 tide (represented by the black arrow) is the vectorial composition of the astronomical K_2 tide (represented by the red arrow) and non-astronomical K_2 tide (represented by the blue arrow) at Mald station. The green arrow represents the modeled K_2 tidal vector (using the FES2014 tide model) in the CM frame. b. Similar distribution in the CF frame, but we use the EOT11a tide model to represent the modeled K_2 tidal vector.

(represented by the green arrow). While the amplitude and phase lag of non-astronomical K_2 constituent are 2.25 mm and 342.4° in the CM frame, and 2.28 mm and 339.9° in the CF frame, respectively. It is shown that although the tidal frequencies of non-astronomical K_2 tide and astronomical K_2 tide are the same, the amplitudes and phase lags characteristics are significantly different due to their different origins and processes.

Similarly, Figs 5 and 6 display the tidal admittances of the semi-diurnal VDL tide at the Pre2 GPS station in the CM frame and in the CF frame. The calculation principle is the same with the Mald GPS station. Via the interpolation, the amplitude and phase lag of the astronomical K_2 constituent at the Pre2 GPS station can be obtained as 2.37 mm and 252.9° in the CM frame, as 2.34 mm and 255.5° in the CF frame, respectively. Figure 7 displays the observed K_2 amplitude and phase lag at the Pre2 GPS station are 1.78 mm and 232.9° in the CM frame, and 1.85 mm and 236.6° in the CF frame, respectively. The amplitude and

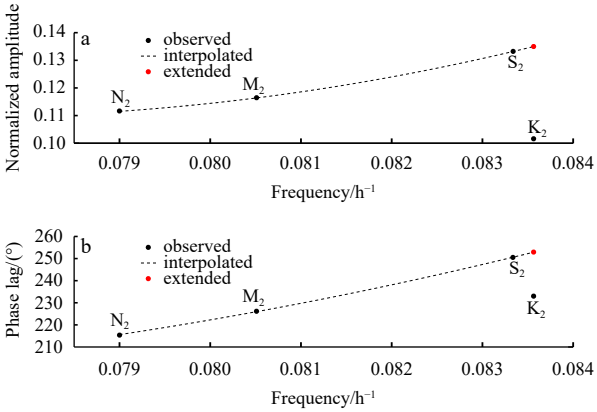

Fig. 5. Tidal admittances of the semi-diurnal VDL tide at Pre2 station in the CM frame. a. Distribution between normalized amplitudes and the frequency of semi-diurnal constituents. b. Distribution between phase lags and the frequency of semi-diurnal constituents. Black dots signify the observed tidal admittances while the dashed lines indicate the interpolated curves. Red dots denote the extended K_2 values based on the interpolated curves.

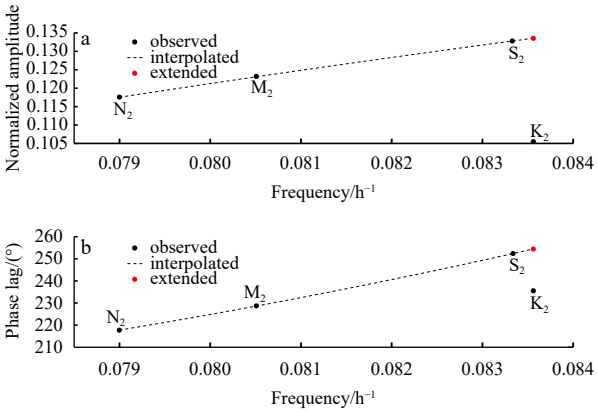

Fig. 6. Tidal admittances of the semi-diurnal VDL tide at Pre2 station in the CF frame. a. Distribution between normalized amplitudes and the frequency of semi-diurnal constituents. b. Distribution between phase lags and the frequency of semi-diurnal constituents. Black dots signify the observed tidal admittances while the dashed lines indicate the interpolated curves. Red dots denote the extended K_2 values based on the interpolated curves.

phase lag of the astronomical K_2 constituent are 2.37 mm and 252.9° in the CM frame, and 2.34 mm and 255.5° in the CF frame, respectively. Figure 7 clearly indicates that the astronomical K_2 tide is highly consistent with the modeled K_2 tide (represented by the green arrow). The amplitude and phase lag of non-astronomical K_2 constituent are 0.92 mm and 114.2° in the CM frame, and 0.84 mm and 120.9° in the CF frame, respectively.

Further, we correct K_2 tide for OTL vertical displacement estimates at 31 GPS stations (Fig. 1) in the CM and CF frame which was provided by Yuan et al. (2013). The corrected harmonic constants of K_2 at 31 GPS stations for the equatorial and Indian Ocean are shown in Table 4.

4.2 *Comparisons with model results*

The amplitude and phase of the GPS gauge considered in this section were obtained from 31 stations (Fig. 1). The harmonic

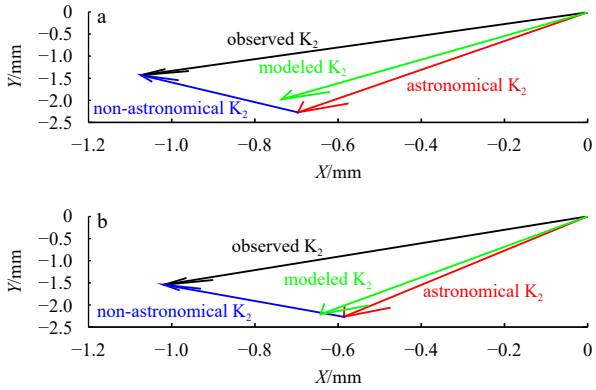

Fig. 7. Vectorial composition of K_2 constituent of VDL tide. a. Observed K_2 tide (represented by the black arrow) is the vectorial composition of the astronomical K_2 tide (represented by the red arrow) and non-astronomical K_2 tide (represented by the blue arrow) at Pre2 station. The green arrow represents the modeled K_2 tidal vector (using the FES2014 tide model) in the CM frame. b. Similar distribution in the CF frame, but we use the EOT11a tide model to represent the modeled K_2 tidal vector.

constants of 31 stations were extracted from each tide model using the spline interpolation method. Then, the harmonic constants for M_2, S_2, N_2, K_2, K_1, O_1, P_1, and Q_1 tidal constituents of tide models (FES2014, EOT11a, GOT4.10c, GOT4.8, and NAO. 99b) were compared with corresponding values of 31 GPS gauge stations (Section 2.2).

The comparison results of the five VDL tide models are listed in Table 5. As is described in Table 5, the discrepancies between the VDL tide models and GPS measurements were large for the positions located along the continental coastlines, with the RMS values ranging from 1.30–3.51 mm for the S_2 and K_1 tidal constituents and 0.39–1.79 mm for the M_2 and O_1 tidal constituents. The remaining constituents (i.e., N_2, K_2, Q_1, and P_1) had comparatively lower RMS values of 0.13–1.22 mm. In detail, the FES2014 model had the best results for M_2, N_2, and P_1 constituents for the equatorial and Indian Ocean with the RMS are 0.61 mm, 0.21 mm, and 0.67 mm, respectively; the EOT11a model had the best results for S_2, K_2, O_1, and Q_1 constituents for the equatorial and Indian Ocean with the RMS are 1.33 mm, 0.39 mm, 0.39 mm, and 0.13 mm, respectively; the GOT4.10c model had the best results for K_1 constituent for the equatorial and Indian Ocean with the RMS is 1.30 mm. Overall, EOT11a and FES2014 models exhibited the smaller RSS value (2.29 mm and 2.34 mm) of the five VDL tide

Table 4. Corrected harmonic constants of K_2 tidal constituent at 31 GPS stations for the equatorial and Indian Ocean

Name	Latitude	Longitude	CM Frame				CF Frame			
			Raw Amp/mm	Raw Pha/(°)	Corrected Amp/mm	Corrected Pha/(°)	Raw Amp/mm	Raw Pha/(°)	Corrected Amp/mm	Corrected Pha/(°)
ade1	34.73°S	138.65°E	0.73	308.0	0.28	335.1	0.85	291.5	0.33	309.4
ade2	34.73°S	138.65°E	1.96	221.0	0.20	345.7	2.21	223.0	0.38	317.7
bahr	26.21°N	50.61°E	1.44	312.9	1.05	294.6	1.53	316.5	1.03	302.8
bhr1	26.21°N	50.61°E	1.20	298.2	1.05	291.1	1.26	303.5	1.02	299.1
cedu	31.87°S	133.81°E	1.18	281.4	0.82	290.7	1.38	274.4	0.91	310.4
coco	12.19°S	96.83°E	3.49	145.3	2.56	146.5	3.40	148.3	2.51	148.6
dgar	7.27°S	72.37°E	5.83	119.7	4.79	115.8	5.67	120.2	4.72	115.3
hrao	25.89°S	27.69°E	2.31	227.3	2.22	261.0	2.37	230.4	2.22	263.9
iisc	13.02°N	77.57°E	0.56	335.9	0.68	80.6	0.66	330.7	0.68	75.6
karr	20.98°S	117.10°E	2.56	305.6	2.11	311.0	2.69	301.5	2.19	307.1
lhaz	29.66°N	91.10°E	1.16	101.4	0.43	107.2	1.11	98.4	0.44	59.1
mal2	3.00°S	40.19°E	4.03	252.7	3.76	243.9	4.08	254.4	3.67	245.3
mald	4.19°N	73.53°E	2.41	52.0	2.66	104.4	2.35	49.1	2.63	103.2
mali	3.00°S	40.19°E	3.61	253.0	4.77	240.9	3.67	254.8	4.69	242.0
nnor	31.05°S	116.19°E	0.29	3.4	0.20	201.4	0.29	311.2	0.35	224.4
ntus	1.35°N	103.68°E	1.22	112.3	0.37	200.8	1.09	116.1	0.42	211.4
pert	31.80°S	115.89°E	0.17	357.6	0.18	136.0	0.25	285.8	0.20	197.3
pre1	25.75°S	28.22°E	1.82	245.0	2.36	259.3	1.92	248.1	2.35	261.9
pre2	25.75°S	28.22°E	1.78	232.9	2.37	252.9	1.85	236.6	2.34	255.5
rbay	28.80°S	32.08°E	3.68	261.0	4.71	256.2	3.82	262.0	4.71	257.3
rcmn	1.22°S	36.89°E	1.90	303.9	1.78	235.2	2.01	305.2	1.67	238.1
reun	21.21°S	55.57°E	1.34	110.8	0.33	129.4	1.17	112.3	0.24	124.5
sey1	4.67°S	55.48°E	2.91	194.9	2.68	226.4	2.88	197.7	2.62	228.0
suth	32.38°S	20.81°E	2.88	248.4	2.48	249.6	2.99	250.0	2.47	252.0
sutm	32.38°S	20.81°E	2.61	250.4	2.48	248.4	2.72	252.1	2.46	250.9
xmis	10.45°S	105.69°E	1.09	234.5	1.46	221.6	1.27	237.9	1.57	224.1
yar1	29.05°S	115.35°E	0.37	162.2	0.25	134.7	0.46	195.2	0.23	179.3
yar2	29.05°S	115.35°E	0.30	0.1	0.22	197.9	0.31	312.2	0.36	220.5
yar3	29.05°S	115.35°E	0.66	262.4	0.04	118.2	0.91	258.4	0.14	237.5
yarr	29.05°S	115.35°E	1.24	248.8	0.24	147.3	1.49	248.6	0.26	190.5
yibl	22.19°N	56.11°E	0.53	284.4	0.88	329.1	0.60	294.8	0.94	336.5

Note: Amp represents amplitude, Pha represents Greenwich phase-lag.

Table 5. Comparison of GPS observations and tide models for the equatorial and Indian Ocean

Constituent	Metric	Metric value				
		FES2014	EOT11a	GOT4.10c	GOT4.8	NAO.99b
M_2	ΔH/mm	0.38	0.66	0.52	0.51	0.77
	Δg/(°)	4.14	3.10	5.80	6.22	20.21
	RMS/mm	**0.61** ± 0.34	0.90 ± 0.37	0.97 ± 0.21	0.95 ± 0.21	1.79 ± 0.21
	r^2/%	99.78	99.53	99.46	99.47	98.15
S_2	ΔH/mm	1.01	0.80	0.98	1.08	0.88
	Δg/(°)	32.35	14.70	13.20	27.80	33.36
	RMS/mm	1.53 ± 0.15	**1.33** ± 0.13	1.55 ± 0.15	1.67 ± 0.22	1.70 ± 0.10
	r^2/%	95.22	96.28	95.09	94.32	94.14
K_1	ΔH/mm	0.77	0.76	0.76	0.77	1.79
	Δg/(°)	8.49	20.23	8.25	8.81	42.79
	RMS/mm	1.33 ± 0.14	1.34 ± 0.17	**1.30** ± 0.13	1.35 ± 0.10	3.51 ± 0.22
	r^2/%	96.82	95.89	96.97	96.76	78.03
O_1	ΔH/mm	0.24	0.26	0.26	0.26	0.71
	Δg/(°)	6.44	3.38	6.29	5.73	26.86
	RMS/mm	0.49 ± 0.25	**0.39** ± 0.30	0.51 ± 0.25	0.47 ± 0.24	1.76 ± 0.23
	r^2/%	99.02	99.26	98.96	99.10	87.50
N_2	ΔH/mm	0.13	0.15	0.14	0.15	0.25
	Δg/(°)	3.61	2.88	3.14	3.83	16.75
	RMS/mm	**0.21** ± 0.40	0.24 ± 0.32	0.25 ± 0.40	0.26 ± 0.38	0.44 ± 0.18
	r^2/%	99.38	99.18	99.11	99.05	97.21
K_2	ΔH/mm	0.28	0.23	0.29	0.35	0.28
	Δg/(°)	19.37	9.78	16.14	40.51	39.36
	RMS/mm	0.47 ± 0.72	**0.39** ± 0.79	0.52 ± 0.67	0.56 ± 0.63	0.56 ± 0.61
	r^2/%	94.30	96.06	93.10	91.88	91.89
P_1	ΔH/mm	0.41	0.40	0.43	0.43	0.59
	Δg/(°)	11.48	16.76	12.02	12.19	42.94
	RMS/mm	**0.67** ± 0.26	0.69 ± 0.25	0.70 ± 0.22	0.71 ± 0.19	1.22 ± 0.25
	r^2/%	92.80	89.98	92.15	91.86	76.26
Q_1	ΔH/mm	0.08	0.07	0.06	0.07	0.16
	Δg/(°)	6.43	4.08	8.48	6.71	19.28
	RMS/mm	0.15 ± 0.49	**0.13** ± 0.49	0.15 ± 0.48	0.14 ± 0.49	0.35 ± 0.38
	r^2/%	98.36	98.56	98.36	98.56	91.16

Note: Bold font denotes the minimum value of RMS. ΔH is the mean absolute difference value of amplitude, Δg is the mean absolute differvalue of phase, and r^2 is the degree of fit between the model values and the actual observed values. RSSs of the five models are 2.34 mm, 2.29 mm, 2.48 mm, 2.58 mm, and 4.86 mm, respectively.

models, indicating a slightly superior performance.

4.3 *Distribution of VDL tide model*

The VDL cotidal charts for the eight major tidal constituents derived from the EOT11a tide model, which accuracy was relatively high in the equatorial and Indian Ocean regions, are presented in Fig. 8. Notably, the M_2 VDL tide exhibits a peak amplitude exceeding 45 mm in the Mozambique Channel, followed by a secondary maximum of over 40 mm along the northwest coast of Australia, and a third maximum exceeding 35 mm in the central Indian Ocean. As expected, the VDL amplitudes on land are comparatively lower due to the absence of load effects. The distribution patterns of the S_2 VDL tide closely resemble those of the M_2 VDL tide. However, given that the amplitudes of the S_2 ocean tide are inherently smaller than those of the M_2 ocean tide, the S_2 VDL amplitudes are correspondingly lower. The first two maxima amplitudes of the S_2 VDL tide, occurring in the Mozambique Channel and along the northwest coast of Australia, have magnitudes exceeding 23 mm, which are nonetheless smaller than those of the M_2 VDL tide. Similarly, a third maximum with amplitudes over 21 mm is observed in the middle of the Indian Ocean. Phase distributions of both the S_2 and M_2 VDL tides exhibit similarities, with a notable difference being the presence of an amphidromic point for the S_2 VDL tide on the west coast of Australia, whereas the M_2 VDL tide displays a degenerated amphidromic point near the southern Australian landmass. The distribution characteristics of the N_2 VDL tide mirror those of the M_2 VDL tide, with similarly reduced amplitudes due to the smaller amplitudes of the N_2 ocean tide. Furthermore, the K_2 VDL tide exhibits a distribution pattern similar to that of the S_2 VDL tide. Notably, the K_1 VDL tide reaches its peak amplitude in the central Arabian Sea, exceeding 18 mm, while a secondary maximum, surpassing 16 mm, is observed along the northwest coast of Australia. Similarly, the O_1 VDL tide exhibits distribution characteristics akin to the K_1 VDL tide, with the two highest amplitudes occurring in the same regions, albeit with magnitudes of over 9 mm and 10 mm, respectively. However, the amplitudes of the P_1 VDL tide are relatively smaller than those of the O_1 VDL tide, reflecting the corresponding reduction in amplitude compared to the O_1 ocean tide. Likewise, the Q_1 VDL tide shares similar distribution characteristics with the O_1 VDL tide.

4.4 *Limitation of using the GPS observations*

Due to various factors such as inherent errors in the GPS sys-

a. M_2, EOT11a

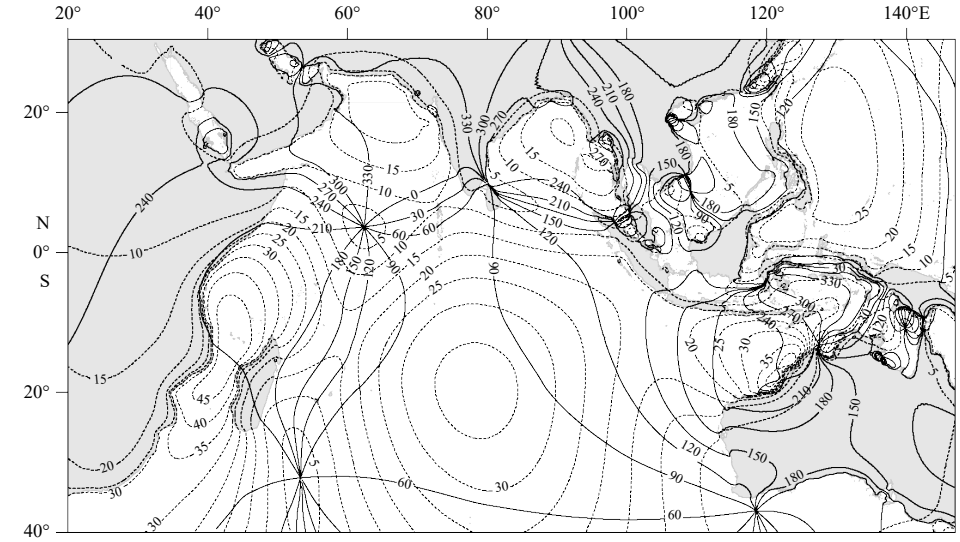

b. S_2, EOT11a

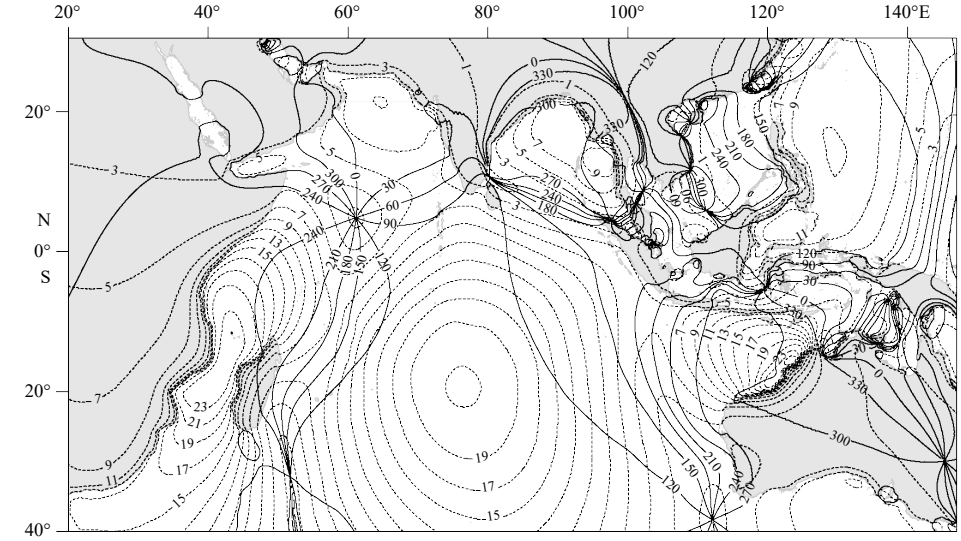

c. N_2, EOT11a

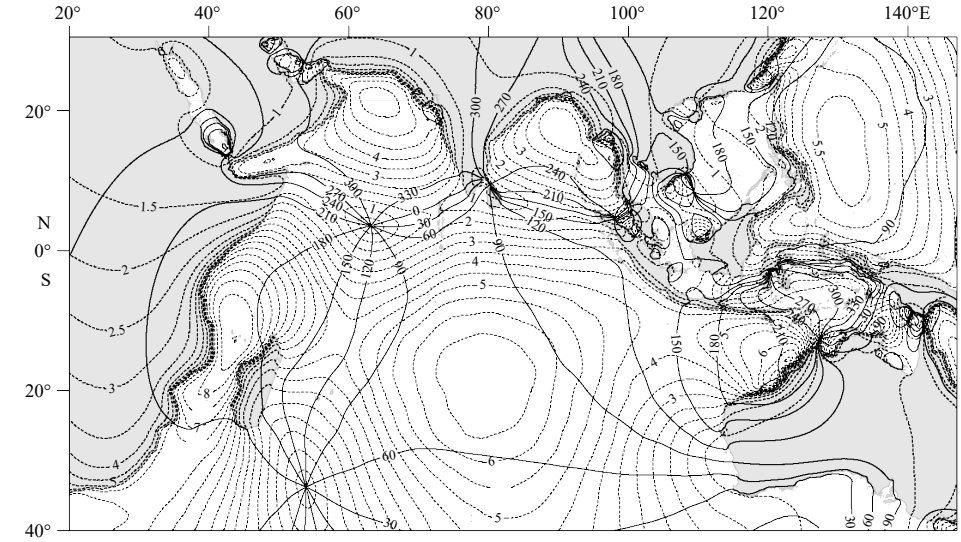

Fig. 8.

d. K_2, EOT11a

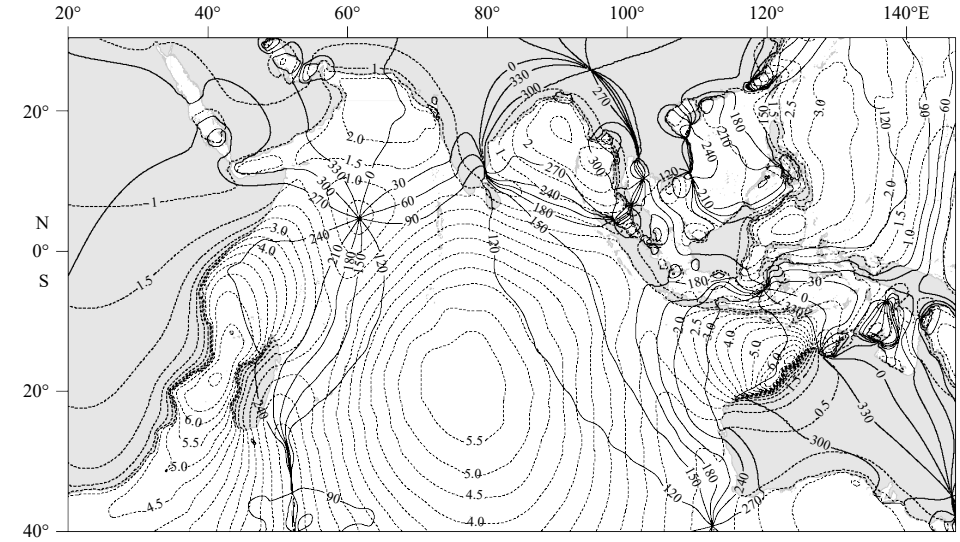

e. K_1, EOT11a

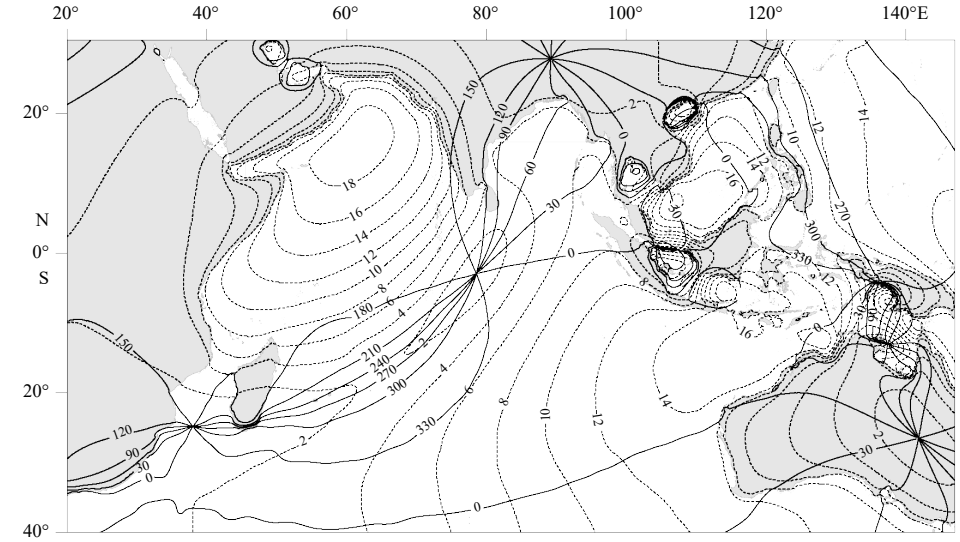

f. O_1, EOT11a

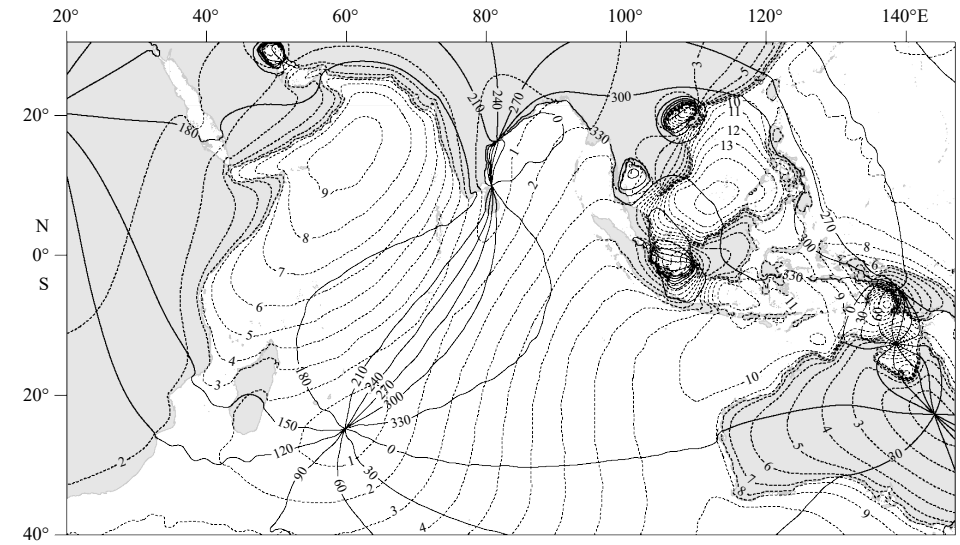

Fig. 8.

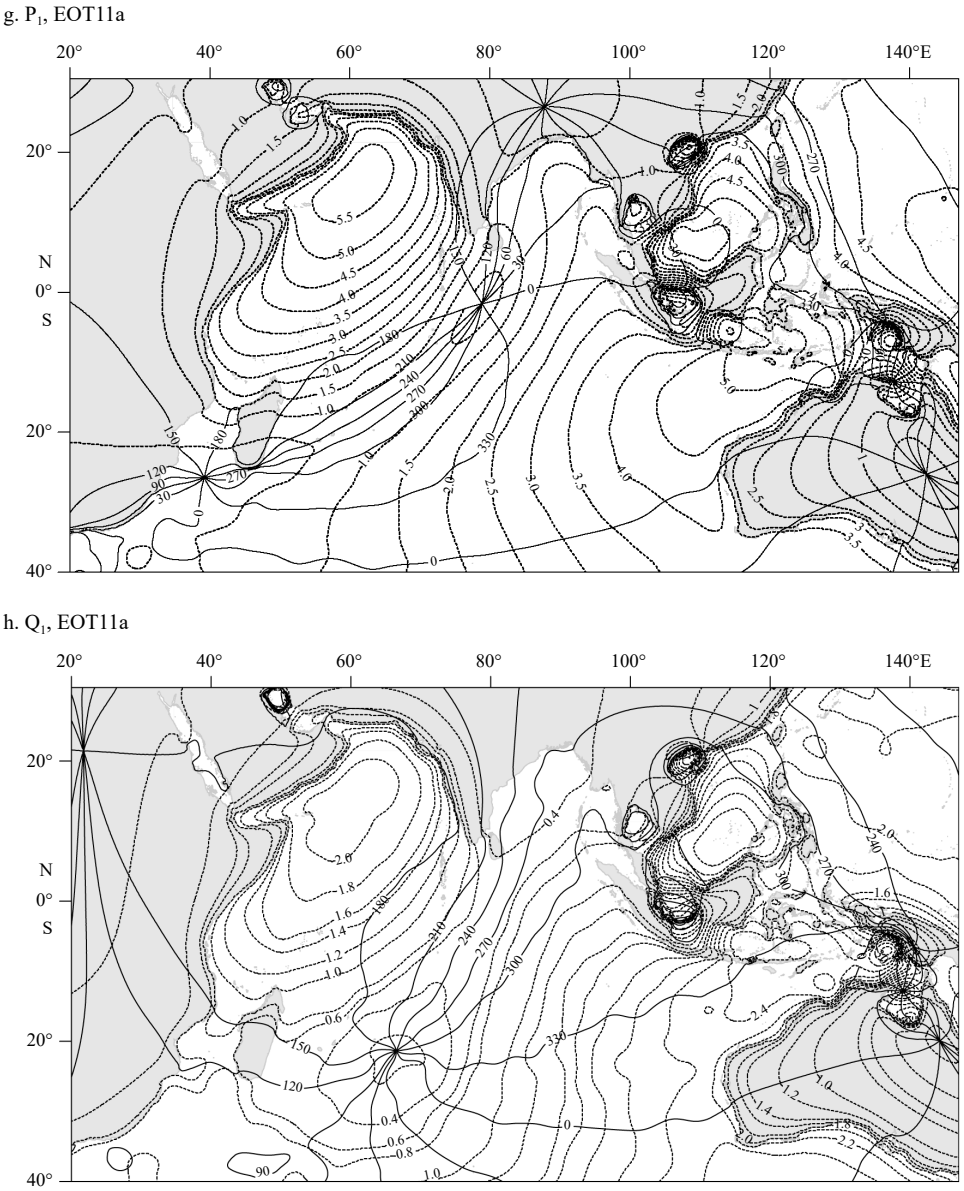

Fig. 8. Co-tidal charts of eight major constituents from EOT11a VDL tide model for the equatorial and Indian Ocean. Dashed lines represent amplitude (mm), solid lines represent Greenwich phase-lag (°).

tem, errors in satellite signal transmission, the complexity of tidal phenomena, and limitations in data processing and analysis methods, tidal constants derived from GPS observations inevitably contain relatively large errors (Table 1). As a consequence, RMSs between GPS results and tidal models have large uncertainties (Table 5), which may exert potential influences on the results of accuracy evaluation. Furthermore, when evaluating the accuracy of VDL models, differences in the number of stations may have potential impacts on the evaluation results, which are all factors that need to be taken into account. It is believed that more effective methods to reduce uncertainties in GPS results will be proposed in the future with the advancement of observation technology.

5 Conclusions

GPS observations can be used to assess the accuracy of the VDL tide models for the equatorial and Indian Ocean due to the displacement deformation of the OTL effect in the North Indian Ocean arises from the circum-North Indian Ocean seas, it also has some disadvantages which can result in significant errors in the estimated K_2 constituent during harmonic analysis. Here, we use the method of tidal admittance smoothing (Pan et al., 2023) to correct the systematic error of the K_2 constituent in GPS observations through quadratic fitting. Based on the comparison of eight tidal constituents (including the corrected K_2 constituent) obtained from GPS observation data, the accuracy of five global vertical displacement tide models (FES2014, EOT11a, GOT4.10c, GOT4.8, and NAO.99b) was assessed for the equatorial and Indian Ocean. As expected, due to the more advanced numerical methods and finer grid resolutions, the EOT11a and FES2014 VDL tide models exhibit higher accuracy for the equatorial and Indian Ocean, with the RMS values ranging from 0.13–1.34 mm and 0.15–1.53 mm for the eight tidal constituents, meanwhile, the RSS values were 2.29 mm and 2.34 mm, respectively. Finally, the distribution characteristics of VDL tides of M_2, S_2, N_2, K_2, K_1, O_1, P_1, and Q_1 major constituents in the study area were briefly ana-

lyzed using the EOT11a model which accuracy was relatively high, the results showed that the maximal amplitudes of M_2 and K_1 VDL tides exceed 45 mm and 18 mm, respectively, indicating that VDL tide is of great significance for the comprehensive understanding of the composition of ocean tides in the North Indian Ocean, as well as in accurately extracting the ocean tides which obtained from satellite altimeter observations.

Acknowlegement

Zexun Wei was supported by the Taishan Scholar Program under contract No. tstp20221148.

References

Aleem A A. 1967. Concepts of currents, tides and winds among medieval Arab geographers in the Indian Ocean. Deep-Sea Research and Oceanographic Abstracts, 14(4): 459–463, doi: 10.1016/0011-7471(67)90052-6

Fang Guohong, Xu Xiaoqing, Wei Zexun, et al. 2013. Vertical displacement loading tides and self-attraction and loading tides in the Bohai, Yellow, and East China Seas. Science China Earth Sciences, 56(1): 63–70, doi: 10.1007/s11430-012-4518-9

Iliffe J C, Ziebart M K, Turner J F, et al. 2013. Accuracy of vertical datum surfaces in coastal and offshore zones. Survey Review, 45(331): 254–262, doi: 10.1179/1752270613Y.0000000040

Ito T, Okubo M, Sagiya T. 2009. High resolution mapping of Earth tide response based on GPS data in Japan. Journal of Geodynamics, 48(3–5): 253–259, doi: 10.1016/j.jog.2009.09.012

Le Provost C L, Lyard F. 1993. Towards a detailed knowledge of the world ocean tides: the example of the Kerguelen Plateau. Geophysical Research Letters, 20(14): 1519–1522, doi: 10.1029/93GL01308

Liu Jingdong, Zhang Wenjing, Liu Chunxiao, et al. 2019. An assessment of tidal prediction by global ocean tide models in the North Indian Ocean. Marine Science Bulletin (in Chinese), 38(2): 159–166, doi: 10.11840/j.issn.1001-6392.2019.02.005

Lyard F H, Allain D J, Cancet M, et al. 2021. FES2014 global ocean tide atlas: design and performance. Ocean Science, 17(3): 615–649, doi: 10.5194/os-17-615-2021

Maraldi C, Galton-Fenzi B, Lyard F, et al. 2007. Barotropic tides of the southern Indian Ocean and the Amery Ice Shelf Cavity. Geophysical Research Letters, 34(18): L18602, doi: 10.1029/2007GL030900

Matsumoto K, Takanezawa T, Ooe M. 2000. Ocean tide models developed by assimilating TOPEX/POSEIDON altimetry data into hydrodynamical model: a global model and a regional model around Japan. Journal of Oceanography, 56(5): 567–581, doi: 10.1023/A:1011157212596

Munk W H, Cartwright D E. 1966. Tidal spectroscopy and prediction. Philosophical Transactions of the Royal Society A: Mathematical, Physical and Sciences, 259(1105): 533–581, doi: 10.1098/rsta.1966.0024

Pan Haidong, Xu Xiaoqing, Zhang Huayi, et al. 2023. A novel method to improve the estimation of ocean tide loading displacements for K_1 and K_2 components with GPS observations. Remote Sensing, 15(11): 2846, doi: 10.3390/rs15112846

Pugh D. 1979. Sea levels at Aldabra Atoll, Mombasa and Mahé, western equatorial Indian Ocean, related to tides, meteorology and ocean circulation. Deep-Sea Research Part A. Oceanographic Research Papers, 26(3): 237–258, doi: 10.1016/0198-0149(79)90022-0

Ray R D. 2013. Precise comparisons of bottom-pressure and altimetric ocean tides. Journal of Geophysical Research: Oceans, 118(9): 4570–4584, doi: 10.1002/jgrc.20336

Savcenko R, Bosch W. 2012. EOT11A-empirical ocean tide model from multi-mission satellite altimetry. München: Deutsches Geodätisches Forschungsinstitut, 49

Seifi F, Deng X L, Baltazar Andersen O. 2019. Assessment of the accuracy of recent empirical and assimilated tidal models for the Great Barrier Reef, Australia, using satellite and coastal data. Remote Sensing, 11(10): 1211, doi: 10.3390/rs11101211

Shum C K, Woodworth P L, Andersen O B, et al. 1997. Accuracy assessment of recent ocean tide models. Journal of Geophysical Research: Oceans, 102(C11): 25173–25194, doi: 10.1029/97JC00445

Visser P N A M, Sneeuw N, Reubelt T, et al. 2010. Space-borne gravimetric satellite constellations and ocean tides: aliasing effects. Geophysical Journal International, 181(2): 789–805, doi: 10.1111/j.1365-246X.2010.04557.x

Wan Rongqiang, Wei Zexun, Gao Xiumin, et al. 2020. Numerical simulation of semi-diurnal tidal waves in the northern Indian ocean. Advances in Marine Science (in Chinese), 38(4): 562–573, doi: 10.3969/j.issn.1671-6647.2020.04.002

Wei Guoguang, Chen Kejie, Ji Run. 2022. Improving estimates of ocean tide loading displacements with multi-GNSS: a case study of Hong Kong. GPS Solutions, 26(1): 25, doi: 10.1007/s10291-021-01212-0

Wei Guoguang, Wang Qijie, Peng Wei. 2019. Accurate evaluation of vertical tidal displacement determined by GPS kinematic precise point positioning: a case study of Hong Kong. Sensors, 19(11): 2559, doi: 10.3390/s19112559

Xu Xiaoqing, Wei Zexun, Teng Fei, et al. 2022. Vertical displacement loading tides and self-attraction and loading tides in the South China Sea and adjacent straits. Haiyang Xuebao (in Chinese), 44(7): 17–24, doi: 10.12284/hyxb2022112

Yuan Linguo, Chao B F, Ding Xiaoli, et al. 2013. The tidal displacement field at Earth's surface determined using global GPS observations. Journal of Geophysical Research: Solid Earth, 118(5): 2618–2632, doi: 10.1002/jgrb.50159

Zetler B D. 1971. Radiational ocean tides along the coasts of the United States. Journal of Physical Oceanography, 1(1): 34–38, doi: 10.1175/1520-0485(1971)001<0032:ROTATC>2.0.CO;2